Environmental Science & Technology

Article

Cite This: Environ. Sci. Technol. XXXX, XXX, XXX−XXX

pubs.acs.org/est

Systematic Comparison of the Influence of Cool Wall versus Cool Roof Adoption on Urban Climate in the Los Angeles Basin

Jiachen Zhang,[†] Arash Mohegh,[†] Yun Li,[†] Ronnen Levinson,[‡] and George Ban-Weiss*[,†]

[†]Department of Civil and Environmental Engineering, University of Southern California, Los Angeles, California 90089, United States

[‡]Lawrence Berkeley National Laboratory, Berkeley, California 94720, United States

Supporting Information

ABSTRACT: This study for the first time assesses the influence of employing solar reflective "cool" walls on the urban energy budget and summertime climate of the Los Angeles basin. We systematically compare the effects of cool walls to cool roofs, a heat mitigation strategy that has been widely studied and employed, using a consistent modeling framework (the Weather Research and Forecasting model). Adoption of cool walls leads to increases in urban grid cell albedo that peak in the early morning and late afternoon, when the ratio of solar radiation onto vertical walls versus horizontal surfaces is at a maximum. In Los Angeles County, daily average increase in grid cell reflected solar radiation from increasing wall albedo by 0.80 is 9.1 W m^{-2}, 43% of that for increasing roof albedo. Cool walls reduce canyon air temperatures in Los Angeles by 0.43 K (daily average), with the peak reduction (0.64 K) occurring at 09:00 LST and a secondary peak (0.53 K) at 18:00 LST. Per 0.10 wall (roof) albedo increase, cool walls (roofs) can reduce summertime daily average canyon air temperature by 0.05 K (0.06 K). Results reported here can be used to inform policies on urban heat island mitigation or climate change adaptation.

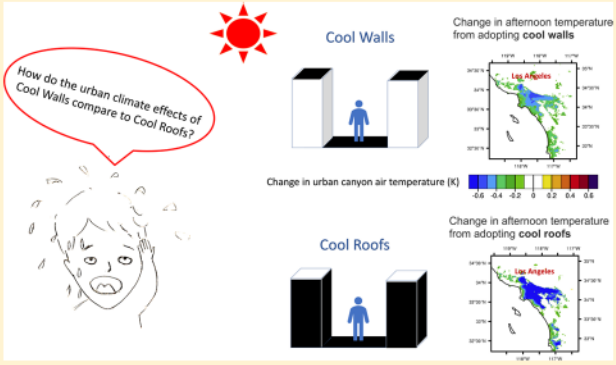

1. INTRODUCTION

The urban heat island effect (UHIE) is a phenomenon in which urban areas are warmer than surrounding rural areas, a result of urban-rural differences in land cover and population density. The UHIE can exacerbate challenges associated with high temperatures in urban areas including (a) human health impacts from extreme heat,[1] such as heat stroke, heat exhaustion rates, and premature deaths; (b) daily total and peak air conditioning energy use during summer;[2] and (c) increases in urban ozone concentrations and potential influences on other air pollutants.[3,4] Several important environmental processes, which are driven by the effects of urban land expansion on surface-atmosphere coupling, can aggravate or mitigate the UHIE. First, widespread application of materials with high solar absorptance (e.g., asphalt concrete and many roofing materials) in urban areas increases absorption of solar energy. Second, extensive use of materials with high heat capacity increases retention of solar energy throughout the day. Third, the geometry of urban canyons (i.e., the space between buildings and above streets) can trap both shortwave (solar) and longwave (thermal infrared) radiation.[5] Fourth, lack of vegetation cover in cities reduces evaporative cooling and shading of the ground surface, thereby increasing urban temperatures.[6] Fifth, increases in soil moisture from irrigation in urban areas can increase evaporative fluxes and cool cities during the day, while at night causing increases in upward ground heat fluxes (due to the increase in soil moisture and thermal conductivity) and therefore nocturnal warming.[7] Sixth, changes in surface roughness from urbanization can also alter wind flows and vertical mixing,[8] with subsequent effects on temperatures that can vary by location. Finally, human activities and industrial processes contribute to releasing waste heat in cities.[9,10]

To lessen the UHIE, heat mitigation strategies have been proposed and employed in some locations to alter the energy balance in cities and decrease temperatures. For example, planting trees and/or adopting vegetative roofs could increase evaporative cooling and reduce urban temperatures.[11] Increasing the albedo, also referred to as solar reflectance (ratio of reflected to incident sunlight) of roofs, walls, and pavements, could reduce solar heat gain, lower surface temperatures, decrease heat transfer from the surface to the atmosphere, and consequently cool the outside air. Heat mitigation strategies can also influence urban climate by changing the hydrological cycle.[12]

The effects of solar-reflective "cool" roofs on urban climate have been well studied in previous research. Large-scale implementation of cool roofs has been predicted to effectively

Received: February 6, 2018
Revised: June 1, 2018
Accepted: August 29, 2018
Published: August 29, 2018

DOI: 10.1021/acs.est.8b00732
Environ. Sci. Technol. XXXX, XXX, XXX−XXX

reduce city-wide air temperatures in Athens, Greece;[13] Sacramento;[14] Baltimore-Washington;[11] and other cities.[15] In Los Angeles, the reduction of peak air temperature induced by increasing both roof and pavement albedo was estimated to reach 1.5 K,[16] while a more recent study[17] estimated the reduction at 13:00 local standard time (LST) in summer to be 0.5 K. In addition, Vahmani et al.[8] concluded that widespread adoption of cool roofs could reduce Southern California summer urban air temperatures by 0.9 K at 14:00 LST and by 0.5 K at 22:00 LST. Santamouris[18] summarized previous literature and concluded that daily average ambient temperatures are expected to decrease linearly with average grid cell albedo increase in cities, declining 0.3 K per 0.1 albedo increase. (We note here that grid cell albedo represents a "bird's eye view" of both impervious and pervious surfaces within modeled urban regions.)

Cool pavements have been studied less than cool roofs. While they are both horizontal surfaces, temperature reductions per unit facet albedo increase can differ between them in part because cool pavements are at the bottom of the urban canyon while roofs are at the top. Mohegh et al.[19] simulated the influence of employing cool pavements on near-surface air temperatures in Californian cities. They found that increasing pavement albedo by 0.40 could lead to annual average air temperature reductions at 14:00 LST ranging by city from 0.19 to 0.87 K. Temperatures at 14:00 LST declined by 0.32 K per 0.10 increase in grid cell average albedo.

Despite previous studies that have examined the effects of raising albedo of horizontal surfaces in different cities, the influence of increasing the albedo of vertical surfaces (e.g., walls) on temperatures has not yet been systematically investigated. The climate effects of increasing wall albedo are expected to differ from those for cool roofs. First, increasing wall albedo and roof albedo by the same amount will influence the energy budget of the urban canopy (i.e., the urban canyon plus roof surfaces) differently for four reasons:

(a) Diurnal cycles of solar irradiance (incident radiative power per unit area) and daily solar irradiation (incident radiative energy per unit area) received by vertical walls differ from those received by (nearly) horizontal roofs. For example, in July, the north, east, south, and west walls of a building in Burbank and Riverside, CA collectively typically receive about 40% as much daily solar irradiation as horizontal roofs (see Tables S5 and S6 in the Supporting Information). Figures S3 and S4 in the Supporting Information compare the diurnal cycle of irradiance on roofs and walls.
(b) Walls make up a different fraction of urban areas than do roofs (see section S1.1 in the Supporting Information for more details).
(c) Walls can be shaded when the sun is low, so the fraction of wall area that is illuminated varies by time of day. In our study, we assume that roofs are not shaded. (In the real-world, nonuniform building heights and trees can lead to roof shading, but we ignore these effects in this study.)
(d) A portion of the solar radiation that is reflected by walls is absorbed by opposing walls and pavements and is thus trapped in the canyon. Solar radiation reflected by roofs, on the other hand, mostly escapes the canopy without being absorbed by other urban facets. Unlike cool roofs, the effect of cool walls depends on the height to width ratio of the urban canopy.

Hence, solar reflections from cool walls differ in timing and magnitude from those from cool roofs.

Second, atmospheric temperature changes induced by cool surfaces are determined not only by the change in the canyon energy budget but also by the diurnal cycle in surface-atmosphere interactions. Diurnal variations in wind speeds, planetary boundary layer (PBL) heights, and atmospheric stability can influence the relationship between changes in the surface energy budget and resulting atmospheric temperature reductions.[20] Cool walls and roofs induce different diurnal cycles in reflected solar radiation. Thus, the diurnal cycles in surface-atmosphere coupling contribute to differences in air temperature change. In other words, even if increases in daily reflected solar radiation were the same for cool walls and roofs, their different diurnal cycles would be expected to lead to different daily average air temperature changes.

Lastly, walls are in the urban canyon, whereas roofs are at the top of the canopy. This means that walls may more directly influence in-canyon air temperatures than roofs, while roofs may more directly influence above-canopy air temperatures.

In this study, we use a regional climate model, coupled to an urban canopy model, to investigate how adopting cool walls would influence albedo, reflection of sunlight, and near-surface air temperature in the Los Angeles basin. We adopt a new parametrization that diagnoses near-surface air temperature within the urban canyon, which is likely more relevant to pedestrian thermal comfort and building energy use than default "2 m air temperature" diagnosed by the model. A suite of additional cool roof simulations systematically compares the climate effects of cool walls to those of cool roofs within a consistent modeling framework.

2. METHODOLOGY

2.1. Model Description. We use the Weather Research and Forecasting model (WRF) version 3.7[21] to investigate the effects of raising wall albedo on near-surface canyon air temperatures in the Los Angeles basin. WRF is developed collaboratively by the National Center for Atmospheric Research (NCAR), the National Oceanic and Atmospheric Administration (NOAA), and other institutes and is widely used to study regional-scale meteorology and climate.

WRF provides several parametrizations that can be used to represent processes that occur at resolutions finer than model grid cells. We summarize here the parametrizations chosen for our simulations. Physics schemes include the Rapid Radiative Transfer Model (RRTM) scheme for long-wave radiation,[22] the Dudhia shortwave scheme[23] for shortwave radiation, the Yonsei University scheme[24] for the planetary boundary layer, and the Lin et al. scheme[25] for cloud microphysics. To simulate cumulus clouds in the middle and outer domains, the Kain-Fritsch convective parametrization is used.[26] The Noah Land Surface Model[27] couples the land surface and atmosphere to compute exchanges in energy (e.g., latent and sensible heat fluxes), momentum, and water. A single-layer urban canopy model (UCM) simulates the influence of urban surface-atmosphere coupling.[28] Parameterizations for physics are chosen to be consistent with our previous modeling studies for Southern California,[7,8,29] which were extensively evaluated by comparing to observations.

The National Land Cover Database for 2006 is used for land cover type classification in the model.[30] For urban grid cells (i.e., cells dominated by urban land cover), we use impervious surface data from the National Land Cover Database

DOI: 10.1021/acs.est.8b00732
Environ. Sci. Technol. XXXX, XXX, XXX−XXX

(NLCD)[31] to compute grid cell specific impervious fractions (i.e., urban fraction, the fraction of each grid cell covered by impervious surfaces). The urban canopy model resolves surface-atmosphere exchange for the impervious part of the grid cell, while the Noah model is used for the pervious portion of urban grid cells. Note that the Noah Land Surface model also handles nonurban grid cells. Urban land use classification and urban morphology will be discussed in section 2.4.

Following Vahmani and Ban-Weiss,[29] we have improved the default version of the WRF model by utilizing MODIS satellite observations to determine grid cell specific green vegetation fraction and leaf area index for pervious areas (i.e., for both the pervious portion of urban grid cells and for nonurban cells). Vahmani and Ban-Weiss found that accounting for high resolution heterogeneity in land surface properties in urban areas can improve model simulations when comparing to observations of meteorology in Los Angeles.

2.2. Shortwave Radiation Calculations in the Urban Canopy Model. In the single-layer urban canopy model (UCM) employed in WRF,[32] the urban canopy is represented as an infinitely long street (a.k.a. ground or canyon floor) bounded by two infinitely long buildings of identical width. That is, there is no separation between adjacent buildings on the same side of the street. Recall that we refer to the urban canopy as the canyon plus roof surfaces.

Direct (beam) and diffuse solar radiation are tracked separately in our model. At solar noon, most beam sunlight strikes horizontal surfaces (roofs and ground), rather than vertical surfaces (walls). In early morning and late afternoon, the ratio of beam vertical radiation to beam horizontal radiation is higher than that at solar noon. Buildings shade the ground when the sun is not at zenith, reducing the ground's solar irradiance and solar heat gain. Since in the canopy model all sunlight not incident on roofs strikes walls or the ground, the beam solar radiation (power) intercepted by the sun-facing wall equals beam horizontal irradiance (power/area) times the length of the ground shadow. Canyon orientation (i.e., the angle between canyon centerline and north) and solar position are considered in the calculations of ground shadow length throughout the day. Eight canyon orientations (0°, 45°, 90°, 135°, 180°, 225°, 270°, 315°) are considered, and the shadow length is averaged among these eight orientations. Ground shadows are longest when the sun is low and shortest when the sun is high. Thus, the fraction of global horizontal irradiance that is incident on the ground peaks at solar noon, while that incident on walls reaches its minimum at solar noon and peaks in the early morning and late afternoon (Figure S4 in the Supporting Information).

The diffuse part of solar radiation can strike all impervious facets (roofs, walls, and ground). Downwelling diffuse solar irradiances on wall and ground surfaces are proportional to the view factors from wall to sky and from ground to sky, respectively. Each facet is assumed to reflect sunlight diffusely. The view factors from ground to wall, from wall to ground, and from sun-facing wall to sun-opposing wall influence the reception of reflected radiation by walls and ground. Note that radiation reflected twice by facets is assumed to fully escape from the urban canopy. For example, absorption within the canopy of light reflected from wall to wall to ground is ignored in the model.

Note that even though WRF-UCM includes a "shadow model" that treats direct and diffuse radiation separately, the default code of WRF-UCM has the "shadow model" turned off. Thus, all solar radiation is treated as diffuse, and shadows casted by buildings are not considered. (See line 853 of module_sf_urban.F in WRF3.7 where SHADOW = .false.) We turn on the shadow calculations by setting SHADOW = .true. We also add to the default shadow model wall-to-wall reflection effects following Kusaka et al.[32]

Downward solar radiation that is not absorbed by roofs, walls, and ground is reflected out of the canopy as upwelling solar radiation. The UCM calculates canopy albedo as the ratio of upwelling sunlight to downwelling sunlight at the horizontal plane bounding the top of the canopy. The changes to canopy albedo upon increasing wall albedo are computed here using the single-layer urban canopy model. Canopy albedo represents the aggregated "above-canopy" albedo of all facets in the urban portion of grid cells, not including contributions from the nonurban portion of the grid cell. Since only the urban portion of the grid cell is modified, changes in grid cell albedo are then computed as change in canopy albedo multiplied by urban fraction (Figure 1c). Note that canopy and grid cell albedo are diagnostic variables and are not used in other model calculations.

2.3. Canyon Air Temperature. For urban grid cells (i.e., grid cells dominated by urban land cover; Figure 1b), the standard WRF diagnoses and outputs canyon temperature and 2-m grid cell air temperature. Canyon temperature is effectively an aggregated skin temperature for walls and ground. This temperature is used in calculations of sensible heat flux from the canyon to the atmosphere. The calculation for the default grid cell 2-m air temperature diagnosed by WRF uses the roughness length of grass, leading to unphysical results in urban grid cells.[33]

To better simulate the temperature near the ground level in cities, we implement the parametrization proposed by Theeuwes et al.[5] to calculate near-surface air temperature within the urban canyon, which we refer to as canyon air temperature. See section S1.2 in the Supporting Information for more details on the canyon air temperature parametrization.

2.4. Urban Land Use Type Classification and Corresponding Canopy Morphology. Urban morphology in the UCM is described by roof width (R), building height (H), and ground width (W). The UCM uses the urban morphology to compute (a) solar irradiance (power/area) incident onto each facet; (b) shortwave radiation (power/area) reflection and longwave radiation (power/area) transfer from each facet to other canyon facets and to the sky; and (c) area weighting factors for averaging solar absorption (power/area) and sensible heat fluxes (power/area) among facets.

Data describing spatially resolved urban morphology from the National Urban Database and Access Portal Tool (NUDAPT) are used where available. NUDAPT data[34] cover only a small portion of our domain but include downtown Los Angeles, where unusually tall buildings are found. For grid cells where NUDAPT data are not available, we derive urban morphology used in this study (Table S1 in the Supporting Information) using data sets as described in section S1.1.

2.5. Simulation Domain. Three nested domains are simulated at resolutions of 18 km, 6 km, and 2 km, respectively (Figure 1a). The outermost domain (d01) covers California; the middle domain (d02) simulates southern California; and the innermost domain (d03) encompasses the Los Angeles basin and San Diego. The domain is the same as that used in our previous modeling work.[7,8,29] Each inner domain uses values from the adjacent outer domain as boundary conditions.

DOI: 10.1021/acs.est.8b00732
Environ. Sci. Technol. XXXX, XXX, XXX−XXX

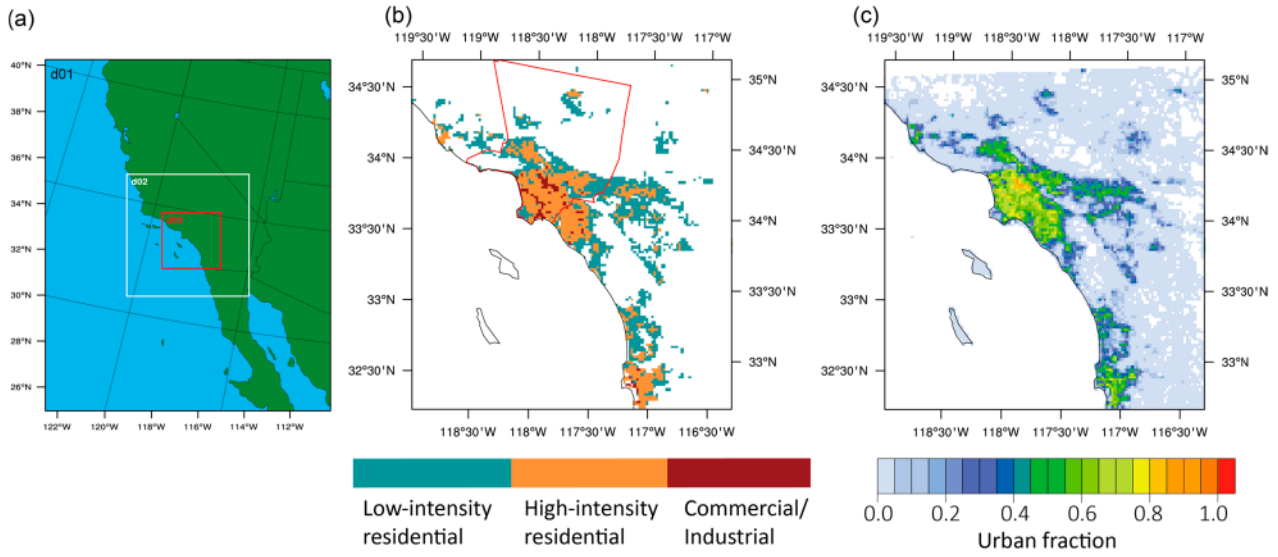

Figure 1. Maps showing (a) the three nested simulation domains d01 (Western United States), d02 (Central and Southern California), and d03 (Southern California), (b) dominant urban land use types for domain d03, where the red outline bounds Los Angeles County considered in our analysis of diurnal air temperatures cycles, and (c) urban fractions in domain d03.

The outermost domain (d1 in Figure 1a) uses the North American Regional Reanalysis (NARR) data set[35] as boundary conditions. The NARR data set has a spatial resolution of 32 km and temporal resolution of 3 h. The atmosphere is simulated using 30 layers in the vertical. Urban areas in Los Angeles County (see Figure 1b) are included in our analysis on diurnal cycles.

2.6. Simulation Design. Our analysis of the influence of cool walls on the climate of Southern California considers three scenarios: CONTROL, in which roof, ground, and wall albedos are all set to 0.10; COOL_WALL_LOW, in which wall albedo is raised to 0.50; and COOL_WALL_HIGH, in which wall albedo is raised to 0.90. To compare the effect of increasing wall albedo to that of raising roof albedo, we add two more scenarios: COOL_ROOF_LOW, in which roof albedo is raised to 0.50; and COOL_ROOF_HIGH, in which roof albedo is raised to 0.90 (Table 1). In this way, the modified-facet albedo increases are 0.40 for COOL_WALL_LOW and COOL_ROOF_LOW scenarios and 0.80 for COOL_WALL_HIGH and COOL_ROOF_HIGH scenarios. Note that cool surface albedos in cases COOL_WALL_HIGH (wall albedo 0.90) and COOL_ROOF_HIGH (roof albedo 0.90) are higher than those of actual cool walls and roofs, especially after weathering and soiling. For example, the albedo of an initially bright-white roof might fall to about 0.60−0.70 from about 0.80−0.90 after several years of exposure.[36,37] The initial albedo of a nonwhite cool surface, such as a "cool colored" roof, typically ranges from about 0.25 to about 0.50,[38] and its albedo loss upon exposure tends to be smaller than that experienced by a bright-white roof.[36] (Section S1.4 in the Supporting Information discusses realistic whole-facet albedo increases that could be attainable from cool wall and cool roof campaigns in Los Angeles.) The albedo values in our simulations are chosen to gauge the upper bound effect of applying cool walls and roofs and to test the linearity of canyon air temperatures with increasing wall and roof albedos. We also simulated an additional scenario that we refer to as COOL_ROOF_WALL_HIGH where the albedos of walls and roofs are both raised to 0.90; this scenario is added to test the linearity of adopting cool walls and roofs simultaneously or separately. Note that the percentage of sunlight reflected by walls that escapes the urban canopy (Table 1) is calculated from urban morphology and wall albedo in section S1.3 in the Supporting Information.

Table 1. Wall and Roof Albedos and the Fraction of Sunlight Reflected by Walls That Escapes the Urban Canopy, for the CONTROL and Four Perturbation Scenarios[b]

scenario	wall albedo	roof albedo	fraction of sunlight reflected by walls that escapes urban canopy (%)[a]
CONTROL	0.10	0.10	50
COOL_WALL_LOW	0.50	0.10	54
COOL_WALL_HIGH	0.90	0.10	59
COOL_ROOF_LOW	0.10	0.50	50
COOL_ROOF_HIGH	0.10	0.90	50

[a]The fraction is constant during daytime for each scenario. [b]Ground albedo is 0.10 in each scenario.

We perform three ensemble simulations per scenario to reduce the influence of model internal variability on results. The ensemble simulations are carried out by initiating the model simulations at different times (13:00 LST on 28 June 2012, 13:00 LST on 29 June 2012, and 13:00 LST on 30 June 2012). Ensemble means are reported for each scenario.

Simulations are performed for 12−14 days (varying by ensemble member) until 00:00 LST, 12 July 2012. Due to intrinsic uncertainties in initial conditions, modeled results at the start of the simulations are unreliable.[39] A previous study with the same model configuration discarded the first 12 simulated hours as model "spin-up".[8] In this study, the first 3 to 5 days (i.e., varying by ensemble member) are discarded as "spin-up", and only the results from 00:00 LST 3 July 2012 to 00:00 LST 12 July 2012 are used in our analysis of changes in canyon air temperatures and albedo.

2.7. Caveats. Note that the results presented in this paper rely on the ability of the model to accurately simulate atmospheric processes and surface-atmosphere interactions. Results may vary depending on the modeling systems employed.

DOI: 10.1021/acs.est.8b00732
Environ. Sci. Technol. XXXX, XXX, XXX−XXX

Also, note that we focus our analysis on Los Angeles County and, accordingly, set the urban canopy morphology and impervious fraction based on region-specific GIS data sets. The climate effects of cool walls and roofs are expected to vary depending on urban morphology and impervious fraction, as well as the baseline climate of the city under investigation.[17,19]

We focus on reductions in air temperatures in this study, but the adoption of cool walls may also bring cobenefits and unintended penalties. Regarding penalties, solar reflective cool walls may lead to increased reflection onto pedestrians, causing glare and reducing their thermal comfort. Levinson et al.[40] examined the colors of cool wall products and their effects on pedestrian thermal comfort. They found that wall albedos of about 0.60 to 0.70 could be attained using readily available off-white or dull-white exterior wall paints with CIELAB lightness (L*) values around 85 (scale 0−100). Simulations with the Temperature of Urban Facets Indoor-Outdoor Building Energy Simulator (TUF-IOBES) model predicted that in Los Angeles, raising wall albedo to 0.60 (cool wall) from 0.25 (conventional wall) would increase the annual average daytime mean radiant temperature of a near-wall pedestrian by about 1 K and increase her annual average daytime standard equivalent temperature (SET*) by about 0.5 K. Cool roofs, on the other hand, are not very likely to lead to these unintended consequences. Policymakers should consider all the aforementioned factors when they plan to adopt cool surfaces.

3. RESULTS AND DISCUSSION

3.1. Diurnal Cycle of Grid Cell Albedo and Reflected Solar Radiation. Figure 2a shows the diurnal cycle of albedo changes induced by cool walls averaged over urban grid cells in Los Angeles County. Figure 2a shows that during the daytime, the urban grid cell albedo rise induced by increasing wall albedo to 0.90 from 0.10 (COOL_WALL_HIGH − CONTROL) is smallest (0.02) at solar noon and greatest (~0.10) in the early morning (06:00 LST) and late afternoon (18:00 LST) in Los Angeles County. (The average sunrise and sunset times for our analysis period are 04:48 LST and 19:07 LST, respectively.) Grid cell albedo increases at 18:00 LST are observed to be similar to the increases at 06:00 LST. This diurnal cycle occurs because wall albedo has its maximum influence on grid cell albedo in the early morning and late afternoon as the ratio of solar irradiance on vertical surfaces versus horizontal surfaces reaches its maximum (Figures S3 and S4 in the Supporting Information). On the other hand, increasing roof albedo by 0.80 (COOL_ROOF_HIGH − CONTROL) will result in a constant urban grid cell albedo rise of 0.07 because the modeled roof is horizontal. Increasing roof albedo, as compared to increasing wall albedo by the same amount, can lead to a greater increase in average urban grid cell albedo in Los Angeles County from 07:00 to 17:00 LST.

Figure 2b shows the diurnal cycle of changes in grid cell upflux (upwelling sunlight) reflected through the horizontal plane bounding the urban canopy. The upflux is calculated as the product of downflux (global horizontal irradiance or GHI) and grid cell albedo. GHI peaks at noon (Figure 2c). The increase in upflux induced by cool walls reaches its two greatest values at 10:00 and 15:00 LST, a result of diurnal variations of both GHI and grid cell albedo increase. Therefore, cool walls can reject more sunlight from the urban canopy in the late morning and early afternoon than during other daylight hours. The diurnal cycles of increases in reflected radiation induced by cool roofs are concave down with larger diurnal variations

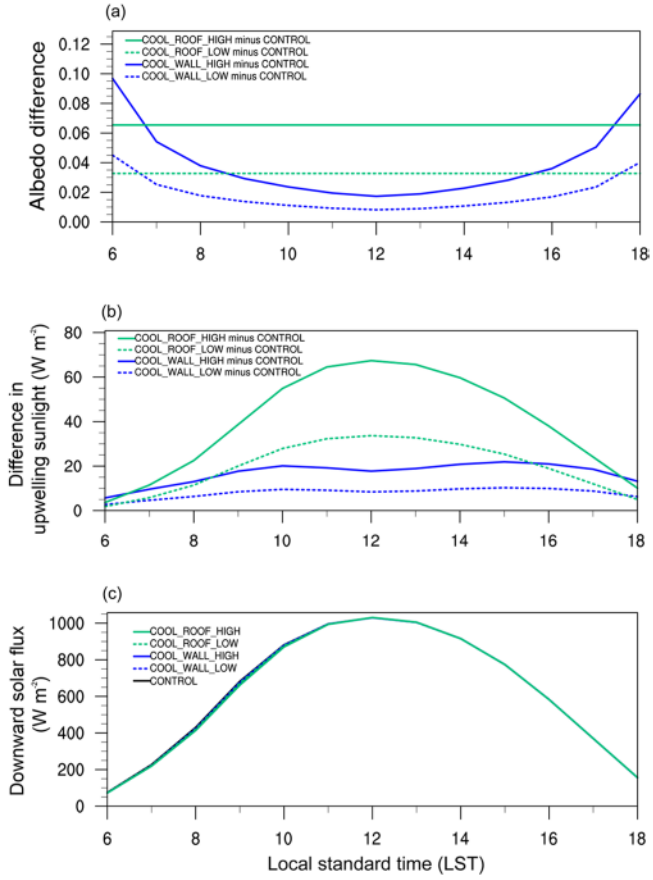

Figure 2. Diurnal cycles of differences between the four perturbation simulations and CONTROL for (a) grid cell albedo and (b) upwelling sunlight, and (c) absolute values for all five scenarios of diurnal cycles of downward solar radiation (global horizontal irradiance). Values represent spatial averages in Los Angeles County (shown in Figure 1b) for urban grid cells averaged over July 3 to 12. Only hours of the day when downward solar flux is greater than 5 W m^{-2} are shown.

relative to cool walls, following the trend of horizontal irradiance (Figure 2c). The increase in solar reflection reaches the maximum at solar noon, the time associated with peak horizontal irradiance.

Relative to CONTROL, the daily average increase in grid cell upflux for COOL_WALL_HIGH (9.1 W m^{-2}) is 43% of that for COOL_ROOF_HIGH (21.3 W m^{-2}) (Table 2). Three factors contribute to the difference in increased reflected solar radiation induced from cool walls versus roofs: (a) gross wall area is a factor of 1.97 greater than roof area in Los Angeles County (section S1.1 in the Supporting Information); (b) solar irradiance (W m^{-2}) onto walls and roofs differ, and daily cumulative solar irradiation (J m^{-2}) onto walls (2,857 J m^{-2}) is 38% of that onto roofs (7,575 J m^{-2}) over the analysis period (Figure S3 in the Supporting Information); and (c) in our model the solar radiation reflected by walls is partially (50−59%) absorbed by walls and pavements (Table 1), while all solar radiation reflected by roofs escapes the canopy.

In our simulations, the increase in wall albedo for COOL_WALL_HIGH − CONTROL (0.80) is twice that for COOL_WALL_LOW − CONTROL (0.40) (Table 1). These wall albedo increases lead to grid cell albedo increases at 06:00 LST and 12:00 LST that differ by a factor of ~2 (Table 2).

DOI: 10.1021/acs.est.8b00732
Environ. Sci. Technol. XXXX, XXX, XXX−XXX

Table 2. Grid Cell Albedo, Grid Cell Solar Upflux (Reflected Solar Radiation),[a] and Canyon Air Temperature at Different Times of Day for Urban Grid Cells in Los Angeles County (Shown in Figure 1b), Including Absolute Values for CONTROL and Changes Relative to CONTROL for the Four Perturbation Scenarios[b]

scenario	albedo at 06:00 LST	albedo at 12:00 LST	daily average solar upflux (W m^{-2})	daily (24-h) average canyon air temp (K)	canyon air temp (K) at 14:00 LST	canyon air temp (K) at 20:00 LST
CONTROL	0.143	0.148	50.2	295.2	302.0	294.5
COOL_WALL_LOW minus CONTROL	0.045	0.008	4.3	−0.19	−0.19	−0.18
COOL_WALL_HIGH minus CONTROL	0.097	0.017	9.1	−0.43	−0.41	−0.40
COOL_ROOF_LOW minus CONTROL	0.033	0.033	10.7	−0.23	−0.34	−0.18
COOL_ROOF_HIGH minus CONTROL	0.065	0.065	21.3	−0.48	−0.72	−0.36

[a]Daily average solar upflux (W m^{-2}) multiplied by 86,400 s (24 h) is equal to daily cumulative solar upflux (J m^{-2}). [b]All values are averages for July 3 to 12.

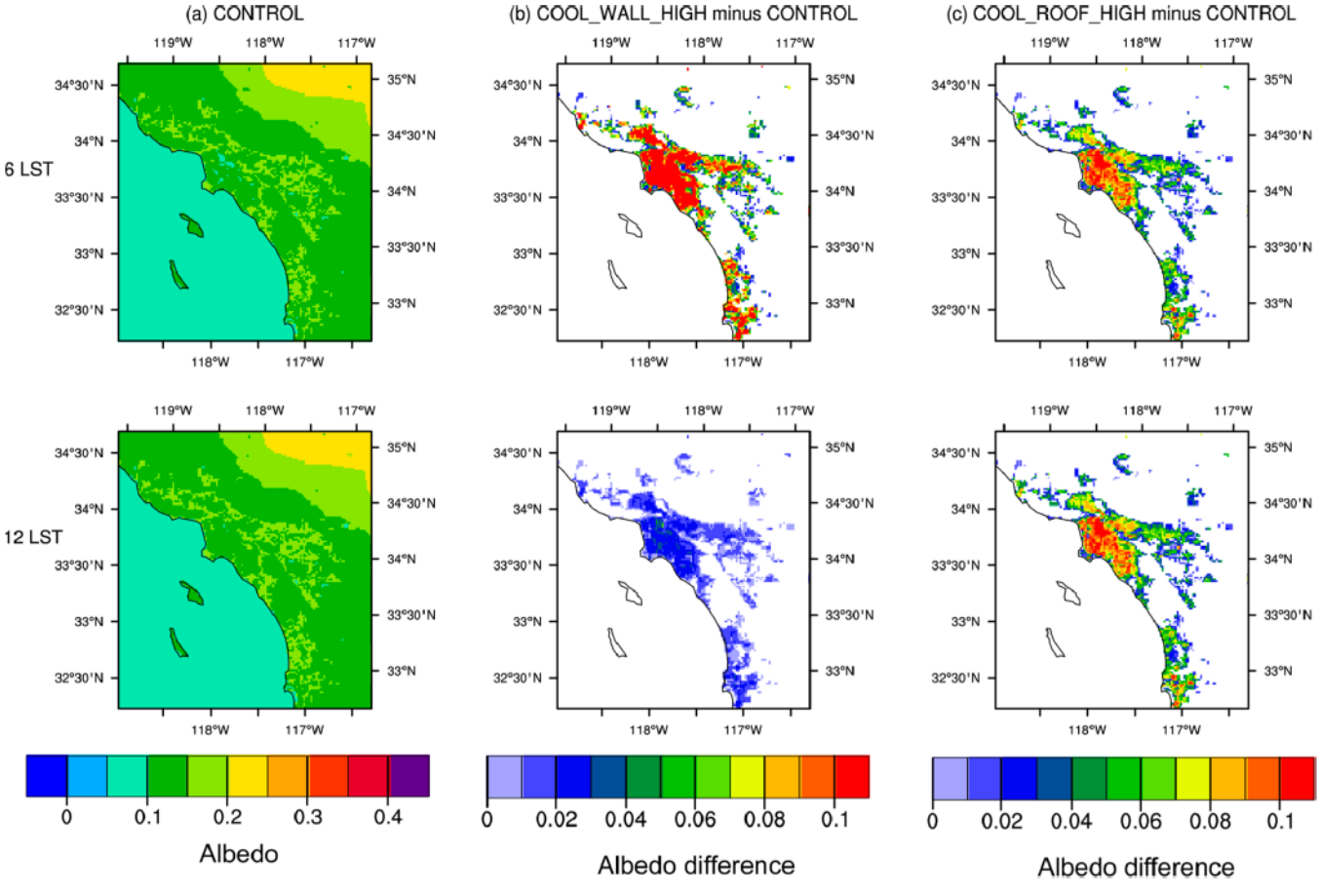

Figure 3. Simulated grid cell albedo at 06:00 LST (top) and 12:00 LST (bottom) for (a) CONTROL, and differences for (b) COOL_WALL_HIGH − CONTROL and (c) COOL_ROOF_HIGH − CONTROL. Values represent averages for July 3 to 12.

This means that the urban increases in grid cell albedo are proportional to wall albedo rises. Similarly, increases in daily cumulative reflected solar radiation scale approximately linearly with wall albedo rise. These linear relationships also apply to cool roofs.

3.2. Spatial Variation of Grid Cell Albedo. Figure 3 shows spatial variations in grid cell albedo for CONTROL (Figure 3a), as well as albedo changes due to raising wall and roof albedos by 0.80 (Figure 3b,c). The spatially resolved albedo increases for 06:00 and 12:00 LST are shown because these times represent when the minimum and maximum albedo increases for cool wall adoption occur (Figure 2a), respectively. Spatial variability in grid cell albedo increase (Figure 3b,c) is caused by spatial variation in urban fraction (Figure 1c) and urban canyon morphologies. Urban grid cells with higher urban fraction (Figure 1c) tend to have larger albedo increases after implementing cool walls or roofs. For example, the albedo increases for COOL_WALL_HIGH − CONTROL in downtown Los Angeles can reach as high as 0.24 at 06:00 LST, which is larger than the spatial average over urban grid cells (0.10). Consistent with Figure 2, the grid cell albedo increase from adopting cool walls is larger at 06:00 than at 12:00 LST. At 06:00 LST (12:00 LST), the grid cell albedo increase induced by adopting cool walls is larger

DOI: 10.1021/acs.est.8b00732
Environ. Sci. Technol. XXXX, XXX, XXX−XXX

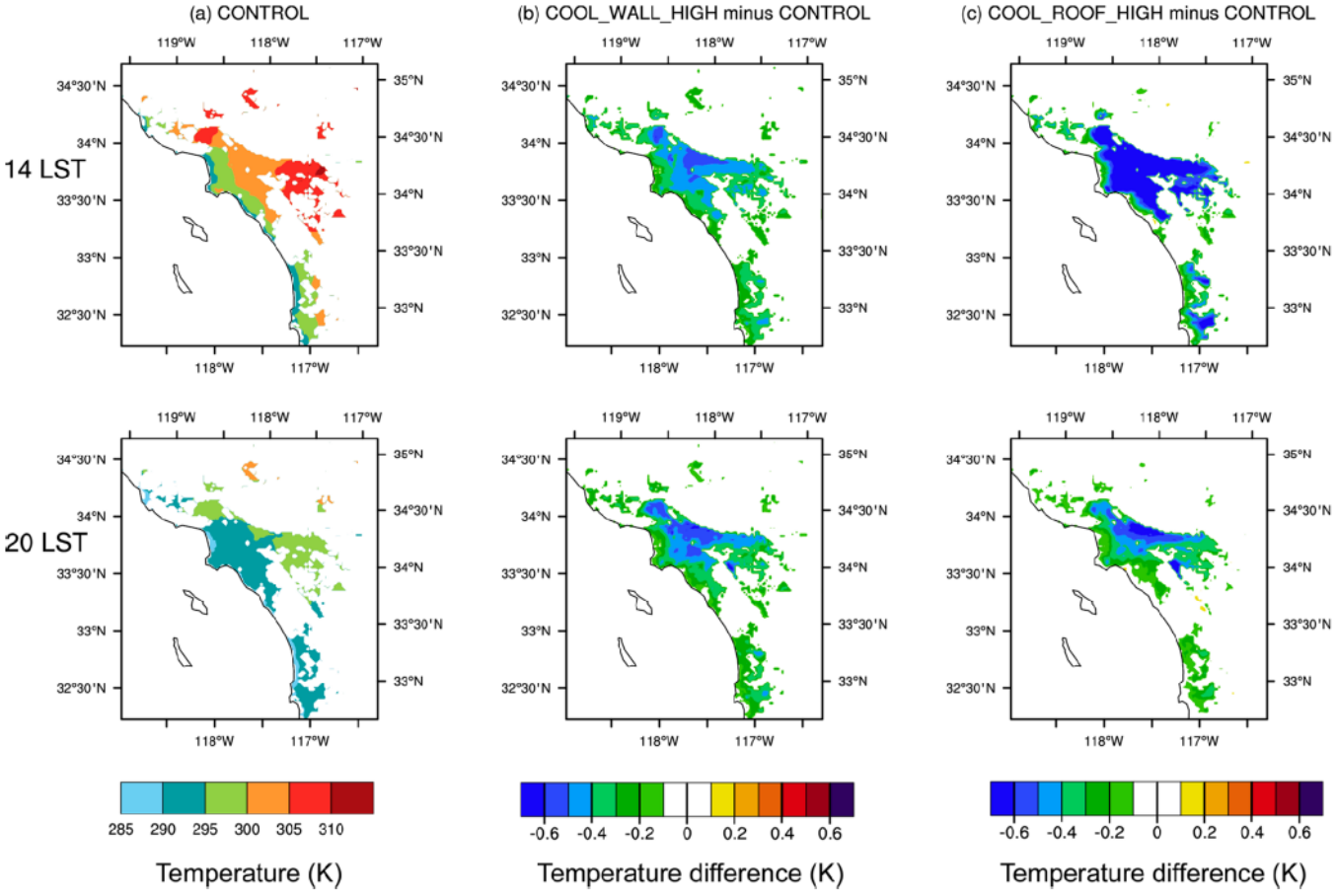

Figure 4. Simulated canyon air temperature (K) at 14:00 LST (top) and 20:00 LST (bottom) for (a) CONTROL, and differences for (b) COOL_WALL_HIGH − CONTROL and (c) COOL_ROOF_HIGH − CONTROL. Values represent averages for July 3 to 12.

(smaller) than that induced by cool roofs with the same facet albedo rise.

3.3. Spatial Variation of Canyon Air Temperatures. Figure 4 shows spatial variation in canyon air temperatures for the control, cool wall, and cool roof simulations at 14:00 LST (daytime) and 20:00 LST (nighttime). In CONTROL, desert regions and the eastern portion of the Los Angeles basin are hotter than the coastal regions, as expected. Employing cool walls and cool roofs reduces temperatures in the urban portions of the domain. Air temperature decreases in inland urban areas are larger than those in coastal areas. This is likely because the effects of cool walls and roofs accumulate as winds (which in Los Angeles are primarily due to sea breeze) advect air from west to east. Cool walls lead to similar canyon air temperature reductions at 14:00 LST and 20:00 LST, while cool roofs cause larger temperature reductions at 14:00 LST than at 20:00 LST. Adopting cool walls shows a greater cooling effect than cool roofs with the same albedo rise relative to CONTROL at 20:00 LST but a smaller cooling effect at 14:00 LST (Figure 4 and Table 2). We discuss the temporal variation of temperature reductions in section 3.4.

3.4. Diurnal Cycle of Canyon Air Temperatures. Figure 5 shows the diurnal cycle of canyon air temperatures for each simulation and changes in temperatures upon raising wall or roof albedo, spatially averaged over the urban regions of Los Angeles County. Figure 5a shows that in each scenario, canyon air temperature reaches its maximum at 13:00 LST. Peak (greatest) air temperature reduction for cool walls (i.e., 0.65 K for COOL_WALL_HIGH − CONTROL and 0.28 K

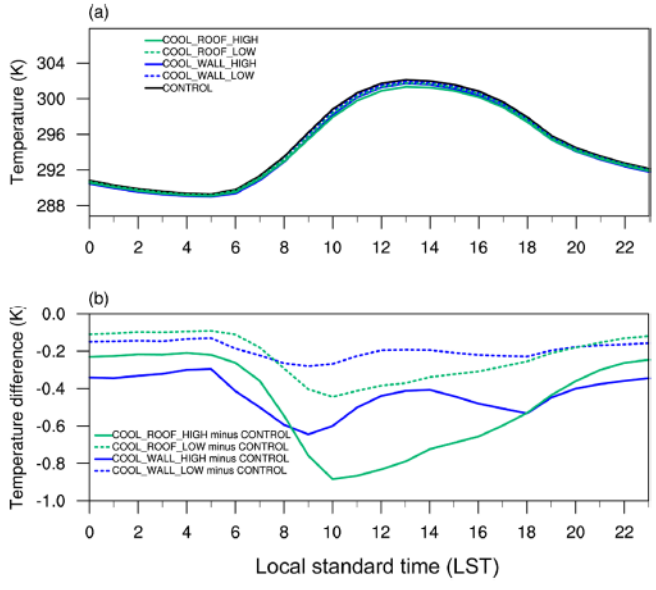

Figure 5. Diurnal cycle of (a) spatially averaged canyon air temperature (K) for CONTROL, COOL_WALL_LOW, COOL_WALL_HIGH, COOL_ROOF_LOW, and COOL_ROOF_HIGH and (b) differences in canyon air temperatures for COOL_WALL_LOW − CONTROL, COOL_WALL_HIGH − CONTROL, COOL_ROOF_LOW − CONTROL, and COOL_ROOF_HIGH − CONTROL. Values represent spatial averages in Los Angeles County (i.e., shown in Figure 1b) for urban grid cells between July 3 and 12.

DOI: 10.1021/acs.est.8b00732
Environ. Sci. Technol. XXXX, XXX, XXX−XXX

for COOL_WALL_LOW − CONTROL) occurs at 09:00 LST (Figure 5b). There is a second (smaller) peak in air temperature reduction observed at 18:00 LST. We hypothesize three factors contributing to the shape of the simulated diurnal cycles for canyon air temperature changes due to cool wall adoption. First, increases in reflected solar radiation and reductions in solar heat gain induced by cool walls are greatest at 10:00 and 15:00 LST (Figure 2b). Second, increasing albedo leads to solar heat gain reductions that accumulate throughout the day. Reductions in the surface temperature of thermally massive structures are related to decreases in accumulated, rather than instantaneous, solar heat gain. Third, the height of the planetary boundary layer (PBL) has a diurnal cycle that is concave down, with a maximum occurring at ~13:00 LST (Figure S5 in the Supporting Information). Shallower PBL heights reduce the volume of air heated by sensible heat fluxes. This means that a given reduction in sensible heat flux caused by surface temperature decreases would lead to larger reductions in atmospheric heating rate (temperature/time) in the boundary layer when PBL heights are shallow versus deep. Thus, sensible heat flux decreases from cool wall adoption are expected to have larger air temperature effects when the PBL is shallow. (Previous research has highlighted the importance of the diurnal cycle in PBL height in determining urban air temperatures; for example, higher PBL heights in urban areas relative to rural areas can contribute to a morning urban cool island.[41] While this study is not directly related to our research, it shows how PBL height can influence atmospheric heating and air temperature in urban areas.)

Section S2.1 in the Supporting Information considers how PBL height, increase in upflux, and the accumulation of solar heat gain affect diurnal cycles of canyon air temperature reduction from adopting cool walls and cool roofs. All three factors contribute to the fact that the greatest reduction in canyon air temperature induced by cool walls occurs at 09:00 LST, which is 1 h before wall irradiance peaks and a time at which the PBL height is relatively low. The second peak occurs at 18:00 LST due to the accumulation effect of reductions in solar heat gain and relatively low PBL height.

For cool roofs, the peak temperature reduction of 0.88 K (COOL_ROOF_HIGH − CONTROL) occurs at 10:00 LST. This peak temperature reduction occurs later in the morning than for cool walls because of the difference in diurnal cycle of increased reflected solar radiation (Figure 2b), which reaches its maximum at solar noon for roofs rather than in the morning and afternoon for walls. A previous study on cool pavements[19] also found that near-surface air temperature reductions peaked in the morning and the evening. They hypothesized that it was due to the combined effects of diurnal cycles in solar irradiance, accumulated solar heat gain, and PBL height.

From 09:00 to 17:00 LST, the canyon air temperature reduction induced by cool roofs is greater than that from cool walls (Figure 5b). This can be attributed to the higher increase in reflected solar radiation that escapes the urban canopy from cool roofs versus walls. However, cool walls (relative to cool roofs) create higher canyon air temperature reductions per increase in reflected solar radiation from the canopy at most times of day (Figure S6 in the Supporting Information). This is likely because walls are in the urban canyon, so they can more directly cool canyon air than roofs. In addition, cool walls lead to a greater cooling at night relative to cool roofs. The atmosphere is stable at night, meaning that there is little vertical mixing. This means that above-canopy air temperature reductions from cool roofs would undergo less mixing into the canyon and thus have less effect on canyon air temperatures relative to cool walls at night.

As shown in Table 2, canyon air temperature reductions for COOL_WALL_HIGH relative to CONTROL at 14:00 and 22:00 LST are about the same (0.41 and 0.40 K, respectively). The reduction at 14:00 LST is lower than that induced by cool roofs (0.72 K), while the reduction at 22:00 LST is higher than that induced by cool roofs (0.36 K). Increasing wall albedo by 0.40 and 0.80 reduces daily average canyon air temperatures by 0.19 and 0.43 K, respectively. In Los Angeles County, the daily average temperature reductions induced by cool walls are slightly less than those induced by cool roofs with the same facet albedo increase. On the other hand, for a daily cumulative grid cell upflux increase of 1 J m^{-2}, the daily canyon temperature reduction induced by cool walls would be 0.55 μK, higher than by cool roofs (0.26 μK).

The ratio of the daily average temperature reduction for COOL_WALL_HIGH − CONTROL to that for COOL_WALL_LOW − CONTROL (0.43 K/0.19 K = 2.3) is close to the ratio of the wall albedo rises for the two scenarios (0.80/0.40 = 2) (Table 2), indicating that the average temperature reduction induced by cool walls is approximately proportional to the increase in wall albedo. A similar linear relationship between facet albedo increase and temperature reduction is also observed for cool roofs (0.48 K/0.23 K = 2.1). Adopting cool walls (roofs) leads to 0.05 K (0.06 K) daily canyon air temperature reduction per 0.10 facet albedo increase. As shown in Figure S7 and Table S7 in the Supporting Information, the reduction in canyon air temperature in COOL_ROOF_WALL_HIGH is approximately the sum of the reductions in COOL_WALL_HIGH and COOL_ROOF_HIGH relative to CONTROL. This suggests that the effects of adopting cool walls and roofs are linear. Thus, results reported here can be interpolated to estimate the effects of increasing wall and/or roof albedo by other amounts.

Canyon air temperature reductions from adopting cool walls or roofs in the Los Angeles basin reported in this study can be used to inform policymaking for urban heat island mitigation or climate change adaptation.

■ ASSOCIATED CONTENT

Supporting Information

The Supporting Information is available free of charge on the ACS Publications website at DOI: 10.1021/acs.est.8b00732.

Method description and further details of results (PDF)

■ AUTHOR INFORMATION

Corresponding Author

*Phone: 213-740-9124. E-mail: banweiss@usc.edu.

ORCID

George Ban-Weiss: 0000-0001-8211-2628

Notes

The authors declare no competing financial interest.

■ ACKNOWLEDGMENTS

This research was supported by the California Energy Commission under contract EPC-14-010 and the National Science Foundation under grants CBET-1512429 and 1752522. This work was also supported by the Assistant Secretary for Energy Efficiency and Renewable Energy,

DOI: 10.1021/acs.est.8b00732
Environ. Sci. Technol. XXXX, XXX, XXX−XXX

Building Technologies Office of the U.S. Department of Energy under Contract No. DE-AC02-05CH11231. Computation for the work described in this paper was supported by the University of Southern California's Center for High-Performance Computing (hpcc.usc.edu). We thank Pablo Rosado for providing calculations on solar irradiance incident to surfaces with different orientations and window-to-wall ratios for different building prototypes. We also thank Gert-Jan Steeneveld, Pouya Vahmani, Dan Li, Ravan Ahmadov, Stu McKeen, Trevor Krasowsky, Mo Chen, Mohammad Taleghani, Wei Tao, Joachim Fallmann, Haley Gilbert, Jan Kleissl, and Junfeng Liu for their helpful suggestions.

REFERENCES

(1) Palecki, M. A.; Changnon, S. A.; Kunkel, K. E. The Nature and Impacts of the July 1999 Heat Wave in the Midwestern United States: Learning from the Lessons of 1995. *Bull. Am. Meteorol. Soc.* **2001**, *82* (7), 1353−1367.

(2) Kolokotroni, M.; Giannitsaris, I.; Watkins, R. The Effect of the London Urban Heat Island on Building Summer Cooling Demand and Night Ventilation Strategies. *Sol. Energy* **2006**, *80* (4), 383−392.

(3) Tao, W.; Liu, J.; Ban-Weiss, G. A.; Zhang, L.; Zhang, J.; Yi, K.; Tao, S. Potential Impacts of Urban Land Expansion on Asian Airborne Pollutant Outflows. *J. Geophys. Res.* **2017**, *122* (14), 7646−7663.

(4) Tao, W.; Liu, J.; Ban-Weiss, G. A.; Hauglustaine, D. A.; Zhang, L.; Zhang, Q.; Cheng, Y.; Yu, Y.; Tao, S. Effects of Urban Land Expansion on the Regional Meteorology and Air Quality of Eastern China. *Atmos. Chem. Phys.* **2015**, *15* (15), 8597−8614.

(5) Theeuwes, N. E.; Steeneveld, G. J.; Ronda, R. J.; Heusinkveld, B. G.; van Hove, L. W. A.; Holtslag, A. A. M. Seasonal Dependence of the Urban Heat Island on the Street Canyon Aspect Ratio. *Q. J. R. Meteorol. Soc.* **2014**, *140* (684), 2197−2210.

(6) Taha, H. Urban Climates and Heat Islands: Albedo, Evapotranspiration, and Anthropogenic Heat. *Energy Build* **1997**, *25* (2), 99−103.

(7) Vahmani, P.; Ban-Weiss, G. Climatic Consequences of Adopting Drought-Tolerant Vegetation over Los Angeles as a Response to California Drought. *Geophys. Res. Lett.* **2016**, *43* (15), 8240−8249.

(8) Vahmani, P.; Sun, F.; Hall, A.; Ban-Weiss, G. Investigating the Climate Impacts of Urbanization and the Potential for Cool Roofs to Counter Future Climate Change in Southern California. *Environ. Res. Lett.* **2016**, *11* (12), 124027.

(9) Fan, H.; Sailor, D. J. Modeling the Impacts of Anthropogenic Heating on the Urban Climate of Philadelphia: A Comparison of Implementations in Two PBL Schemes. *Atmos. Environ.* **2005**, *39* (1), 73−84.

(10) Oke, T. R.; Johnson, G. T.; Steyn, D. G.; Watson, I. D. Simulation of Surface Urban Heat Islands under "ideal" Conditions at Night Part 2: Diagnosis of Causation. *Boundary-Layer Meteorol* **1991**, *56* (4), 339−358.

(11) Li, D.; Bou-Zeid, E.; Oppenheimer, M. The Effectiveness of Cool and Green Roofs as Urban Heat Island Mitigation Strategies. *Environ. Res. Lett.* **2014**, *9* (5), 055002.

(12) Georgescu, M.; Morefield, P. E.; Bierwagen, B. G.; Weaver, C. P. Urban Adaptation Can Roll Back Warming of Emerging Megapolitan Regions. *Proc. Natl. Acad. Sci. U. S. A.* **2014**, *111* (8), 2909−2914.

(13) Synnefa, A.; Dandou, A.; Santamouris, M.; Tombrou, M.; Soulakellis, N. On the Use of Cool Materials as a Heat Island Mitigation Strategy. *J. Appl. Meteorol. Climatol.* **2008**, *47* (11), 2846−2856.

(14) Taha, H. Meso-Urban Meteorological and Photochemical Modeling of Heat Island Mitigation. *Atmos. Environ.* **2008**, *42* (38), 8795−8809.

(15) Zhang, J.; Zhang, K.; Liu, J.; Ban-Weiss, G. Revisiting the Climate Impacts of Cool Roofs around the Globe Using an Earth System Model. *Environ. Res. Lett.* **2016**, *11* (8), 084014.

(16) Rosenfeld, A. H.; Akbari, H.; Romm, J. J.; Pomerantz, M. Cool Communities: Strategies for Heat Island Mitigation and Smog Reduction. *Energy Build* **1998**, *28* (1), 51−62.

(17) Millstein, D.; Menon, S. Regional Climate Consequences of Large-Scale Cool Roof and Photovoltaic Array Deployment. *Environ. Res. Lett.* **2011**, *6* (3), 034001.

(18) Santamouris, M. Cooling the Cities - A Review of Reflective and Green Roof Mitigation Technologies to Fight Heat Island and Improve Comfort in Urban Environments. *Sol. Energy* **2014**, *103*, 682−703.

(19) Mohegh, A.; Rosado, P.; Jin, L.; Millstein, D.; Levinson, R.; Ban-Weiss, G. Modeling the Climate Impacts of Deploying Solar Reflective Cool Pavements in California Cities. *J. Geophys. Res.* **2017**, *122* (13), 6798−6817.

(20) Bonan, G. B. *Ecological Climatology: Concepts and Applications*, 2nd ed.; 2010; Vol. *48*, DOI: 10.1111/j.1745-5871.2009.00640.x.

(21) Skamarock, W. C.; Klemp, J. B.; Dudhi, J.; Gill, D. O.; Barker, D. M.; Duda, M. G.; Huang, X.-Y.; Wang, W.; Powers, J. G. *A Description of the Advanced Research WRF Version 3*; NCAR Technical Note NCAR/TN-475+STR; 2008; No. June, p 113.

(22) Mlawer, E. J.; Taubman, S. J.; Brown, P. D.; Iacono, M. J.; Clough, S. A. Radiative Transfer for Inhomogeneous Atmospheres: RRTM, a Validated Correlated-k Model for the Longwave. *J. Geophys. Res. Atmos.* **1997**, *102* (D14), 16663−16682.

(23) Dudhia, J. Numerical Study of Convection Observed during the Winter Monsoon Experiment Using a Mesoscale Two-Dimensional Model. *J. Atmos. Sci.* **1989**, *46*, 3077−3107.

(24) Hong, S.-Y.; Noh, Y.; Dudhia, J. A New Vertical Diffusion Package with an Explicit Treatment of Entrainment Processes. *Mon. Weather Rev.* **2006**, *134* (9), 2318−2341.

(25) Lin, Y.-L.; Farley, R. D.; Orville, H. D. Bulk Parameterization of the Snow Field in a Cloud Model. *J. Clim. Appl. Meteorol.* **1983**, *22*, 1065−1092.

(26) Kain, J. S. The Kain−Fritsch Convective Parameterization: An Update. *J. Appl. Meteorol.* **2004**, *43* (1), 170−181.

(27) Chen, F.; Dudhia, J. Coupling an Advanced Land Surface−Hydrology Model with the Penn State−NCAR MM5Modeling System. Part II: Preliminary Model Validation. *Mon. Weather Rev.* **2001**, *129* (4), 587−604.

(28) Chen, F.; Kusaka, H.; Bornstein, R.; Ching, J.; Grimmond, C. S. B.; Grossman-Clarke, S.; Loridan, T.; Manning, K. W.; Martilli, A.; Miao, S.; Sailor, D.; Salamanca, F. P.; Taha, H.; Tewari, M.; Wang, X.; Wyszogrodzki, A. A.; Zhang, C. The Integrated WRF/Urban Modelling System: Development, Evaluation, and Applications to Urban Environmental Problems. *Int. J. Climatol.* **2011**, *31* (2), 273−288.

(29) Vahmani, P.; Ban-Weiss, G. Impact of Remotely Sensed Albedo and Vegetation Fraction on Simulation of Urban Climate in WRF-UCM: A Case Study of the Urban Heat Island in Los Angeles. *J. Geophys. Res. Atmos.* **2016**, *121* (4), 1511−1531.

(30) Fry, J. A.; Xian, G.; Jin, S.; Dewitz, J. A.; Homer, C. G.; Yang, L.; Barnes, C. A.; Herold, N. D.; Wickham, J. D. Completion of the 2006 National Land Cover Database for the Conterminous United States. *Photogramm. Eng. Remote Sensing* **2011**, *77*, 858−864.

(31) Wickham, J. D.; Stehman, S. V.; Gass, L.; Dewitz, J.; Fry, J. A.; Wade, T. G. Accuracy Assessment of NLCD 2006 Land Cover and Impervious Surface. *Remote Sens. Environ.* **2013**, *130*, 294−304.

(32) Kusaka, H.; Kondo, H.; Kikegawa, Y.; Kimura, F. A Simple Single-Layer Urban Canopy Model for Atmospheric Models: Comparison with Multi-Layer and Slab Models. *Boundary-Layer Meteorol* **2001**, *101* (3), 329−358.

(33) Li, D.; Bou-Zeid, E. Quality and Sensitivity of High-Resolution Numerical Simulation of Urban Heat Islands. *Environ. Res. Lett.* **2014**, *9* (5), 055001.

(34) Ching, J.; Brown, M.; Burian, S.; Chen, F.; Cionco, R.; Hanna, A.; Hultgren, T.; McPherson, T.; Sailor, D.; Taha, H.; Williams, D. National Urban Database and Access Portal Tool. *Bull. Am. Meteorol. Soc.* **2009**, *90* (8), 1157−1168.

DOI: 10.1021/acs.est.8b00732
Environ. Sci. Technol. XXXX, XXX, XXX−XXX

(35) Mesinger, F.; DiMego, G.; Kalnay, E.; Mitchell, K.; Shafran, P. C.; Ebisuzaki, W.; Jović, D.; Woollen, J.; Rogers, E.; Berbery, E. H.; Ek, M. B.; Fan, Y.; Grumbine, R.; Higgins, W.; Li, H.; Lin, Y.; Manikin, G.; Parrish, D.; Shi, W. North American Regional Reanalysis. *Bull. Am. Meteorol. Soc.* **2006**, *87* (3), 343−360.
(36) Sleiman, M.; Ban-Weiss, G.; Gilbert, H. E.; François, D.; Berdahl, P.; Kirchstetter, T. W.; Destaillats, H.; Levinson, R. Soiling of Building Envelope Surfaces and Its Effect on Solar Reflectance - Part I: Analysis of Roofing Product Databases. *Sol. Energy Mater. Sol. Cells* **2011**, *95* (12), 3385−3399.
(37) Berdahl, P.; Akbari, H.; Levinson, R.; Miller, W. A. Weathering of Roofing Materials - An Overview. *Constr. Build. Mater.* **2008**, *22* (4), 423−433.
(38) Levinson, R.; Berdahl, P.; Akbari, H.; Miller, W.; Joedicke, I.; Reilly, J.; Suzuki, Y.; Vondran, M. Methods of Creating Solar-Reflective Nonwhite Surfaces and Their Application to Residential Roofing Materials. *Sol. Energy Mater. Sol. Cells* **2007**, *91* (4), 304−314.
(39) Warner, T. T. *Numerical Weather and Climate Prediction*; Cambridge, 2011; DOI: 10.1017/CBO9780511763243.
(40) Levinson, R.; Gilbert, H.; Zhang, J.; Ban-Weiss, G.; Kleissl, J.; Pizzicotti, M.; Zhang, W.; Dumas, N.; Kurtz, B.; Long, Y.; Nazarian, N.; Mohegh, A.; Li, Y.; Tang, X.; Chen, S.; Russell, M.; Houzé de, S.; Destaillats, H. *Solar-Reflective "Cool" Walls: Benefits, Technologies, and Implementation*; 2018.
(41) Theeuwes, N. E.; Steeneveld, G. J.; Ronda, R. J.; Rotach, M. W.; Holtslag, A. A. M. Cool City Mornings by Urban Heat. *Environ. Res. Lett.* **2015**, *10* (11), 114022.

DOI: 10.1021/acs.est.8b00732
Environ. Sci. Technol. XXXX, XXX, XXX−XXX